

Alkylamine-mediated synthesis and optical properties of copper nanopolyhedrons

Qi Gao^{1,2} · Caixia Kan¹ · Junlong Li¹ · Jingjing Wei¹ · Yuan Ni¹ · Changshun Wang¹

Received: 19 August 2016 / Accepted: 19 October 2016 / Published online: 27 October 2016
© Springer Science+Business Media Dordrecht 2016

Abstract An alkylamine-mediated hydrothermal synthesis method is proposed for fabrication of copper (Cu) nanopolyhedrons (including tetrahedral and cubic shapes) with well-defined facets and controllable size by modulating the coordination chemistry of a sole ligand (hexadecylamine, HDA) or dual ligands [HDA and octadecylamine (ODA)]. The size of the nanopolyhedrons increases with decreasing HDA/ODA mole ratio. Both the nanocubes and nanotetrahedrons are single-crystal structures, bound by six {100} or four {111} facets, respectively. The complexation reaction temperature plays a vital role in determining the final morphology of the as-prepared nanocrystals. High complexation reaction temperature is suitable for generation of single-crystalline Cu nuclei and their further growth into nanocubes and nanotetrahedrons, while low temperature leads to formation of multitwinned crystal seeds that finally develop into nanowires. Moreover, the probable aggregative growth is discussed to explain the growth mechanism of the Cu nanopolyhedrons. In addition, double surface plasmon resonance peaks are observed in the absorbance spectra for the Cu nanopolyhedrons with relatively large size. Finite-difference time-domain simulations reveal that the experimental absorption spectra are the superposition of those for nanocubes and nanotetrahedrons in different proportions. The peak at about 600 nm in the experimental spectra mainly originates from the Cu nanocubes, while the absorption from 750 to 950 nm derives from the Cu nanotetrahedrons. These angular Cu nanocubes and nanotetrahedrons may have potential applications in surface-enhanced Raman scattering and catalysis.

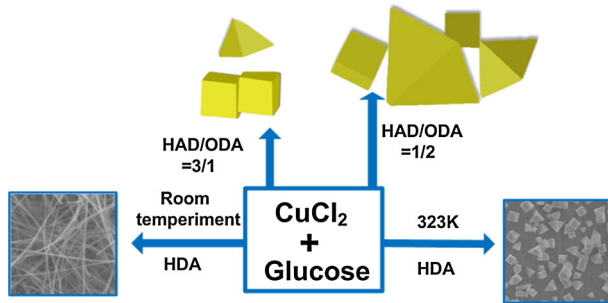
Electronic supplementary material The online version of this article (doi:10.1007/s11164-016-2793-3) contains supplementary material, which is available to authorized users.

✉ Caixia Kan
cxkan@nuaa.edu.cn

¹ College of Science, Nanjing University of Aeronautics and Astronautics, Nanjing 210016, People's Republic of China

² School of Mathematics and Physics, Jiangsu University of Science and Technology, Changzhou 213001, People's Republic of China

Graphical Abstract



Keywords Copper nanocubes · Copper nanotetrahedrons · Alkylamine · Aggregative growth · Plasmon resonance

Introduction

In recent years, copper (Cu) nanostructures have attracted great interest as metal nanomaterials because of their advantages of excellent optical, electrical, thermal, and catalytic properties for use in various applications; For example, Cu nanoparticles have been widely used as catalysts for water–gas shift and gas detoxification reactions [1–4]. Cu nanowires are used for fabrication of high-performance transparent electrodes because of their high conductivity and optical transmittance [5–9]. These transparent electrodes are essential components for touchscreens, solar cells, organic light-emitting diodes, and many other optoelectronic devices. In addition, Cu has the second highest electrical conductivity of all the metals and is more abundant and less expensive compared to gold (Au) and silver (Ag). However, due to the difficulty in reducing Cu ions to metallic Cu and the susceptibility of Cu nanostructures to oxidation upon exposure to air and water, synthesis of Cu nanostructures with high stability and anisotropy remains a challenge [10]. Therefore, extensive research efforts have been made to fabricate Cu nanocrystals with well-defined facets and controllable shape. Although a few such methods have been developed to synthesize uniform Cu nanoparticles [11–15] and nanowires [16–20], efforts to produce well-defined nanostructures with cubic [21], platelet [22], octahedral [23, 24], and other anisotropic morphologies are still ongoing.

In contrast to nanospheres and irregular nanostructures, metallic nanocubes with six identical {100} facets have many special properties; For example, the catalytic activity of platinum (Pt) nanocubes is over two times higher than that of commercial Pt catalysts for oxygen reduction, because Pt {100} planes are more active than the others [25]. In synthesis of Cu nanocubes, selected additives such as NH_4Cl [26], trioctylphosphine (TOP) [27], and trioctylphosphine oxide [21] have proven to be effective for fabrication of cubic morphology. Recently, Yang et al. [28] reported

that truncated Cu nanocubes with average edge length of 75 nm could be synthesized by rapidly injecting a mixture of CuCl and octadecylamine (ODA) into hot oleylamine/TOP solution. Huang et al. [26] utilized NH_4Cl as a shape modifier to direct single-crystalline nuclei into monodispersed cubic nanocrystals with average edge length of 45 nm. Generally, the reported Cu nanocubes with size less than 80 nm are truncated and easily oxidized on the face, whereas there have been few investigations on larger-sized Cu nanocubes with flat faces and sharp edges. In addition, a tetrahedron surrounded by four $\{111\}$ facets is regarded as an effective model to study the special surface properties of such materials. It is stated that different crystal facets have distinct catalytic activities. Nanotetrahedrons with four $\{111\}$ facets, for instance, exhibit better catalytic performance. Gu et al. [29] demonstrated that the $\{111\}$ facets of ruthenium (Ru) nanotetrahedrons were more inert to oxygen adsorption and showed moderate adsorption energy for hydrogen. Moreover, Pt@Ru nanotetrahedrons maximized exposure of $\{111\}$ facets of Ru, leading to greatly enhanced hydrogen oxidation reaction activity on this kind of nanocatalyst. However, only a few methods can synthesize metal nanotetrahedrons with controllable shape and size. To date, the most widely reported example has been Pt nanotetrahedrons [30, 31]. To the best of the authors' knowledge, Cu nanotetrahedrons have not yet been reported.

It is well known that nanocrystal growth is determined by both kinetics and thermodynamics. In this case, solution-phase crystal growth is usually far from the thermodynamic theory in which the final crystal shape is determined such that the total free energy of the system is minimized; rather, the growth rate of each face is determined by kinetics [32]. In particular, capping agents have been widely used to control the growth rate of different crystal facets.

Herein, we present effective strategies (sole or dual ligands) for preparation of Cu nanopolyhedrons (including nanocubes and nanotetrahedrons) with different sizes and well-defined facets. By elevating the complexation reaction temperature and changing the ratio of the ligands, the roles of alkylamines were determined in detail to exploit the growth mechanism of this synthetic system. Finally, theoretical simulations of the absorbance and scattering spectra of the as-prepared Cu nanopolyhedrons were undertaken for better understanding of their optical properties.

Materials and methods

Chemicals

Copper(II) chloride dihydrate (CuCl_2 , AR, SCRC), D-glucose ($\text{C}_6\text{H}_{12}\text{O}_6 \cdot 3\text{H}_2\text{O}$, Reanal), hexadecylamine (HDA: $\text{C}_{16}\text{H}_{35}\text{N}$, Tech 95%), ODA ($\text{C}_{18}\text{H}_{39}\text{N}$, Tech 90%), hexane (C_6H_{14} , Sigma-Aldrich, 96.5%), and ethanol ($\text{C}_2\text{H}_6\text{O}$, Mole Chemical, 99%) were purchased from Shanghai Chemical Reagent Co. Ltd. All reagents were used as received without further purification. Water was purified using a Milli-Q system (Millipore).

Synthesis of Cu nanocubes and nanotetrahedrons

In a typical sole-ligand preparation procedure, 40 mL CuCl_2 aqueous solution (12.5 mM) with $\text{C}_6\text{H}_{12}\text{O}_6$ (25 mM) and HDA (0.632 g) was heated at 323 K for 5 h with strong magnetic stirring to obtain light-blue emulsion. This emulsion was then transferred to a Teflon-lined stainless-steel autoclave with capacity of 60 mL. The autoclave was kept at 393 K for 6 h under autogenous pressure before cooling down to room temperature naturally. Similarly, a typical dual-ligand preparation procedure was carried out according to the above process but substituting HDA with HDA and ODA, while all other parameters were kept the same. The detailed experimental parameters are presented in Table S1. The resulting reddish-brown colloid was centrifuged (at 3000 rpm) and washed with deionized water, hexane, and ethanol, sequentially, to remove excess surfactants. Subsequently, a reddish colloid was obtained and kept in hexane to avoid oxidation of the Cu products.

Characterization

Samples for transmission electron microscopy (TEM) analysis were prepared by dropping Cu nanocrystal suspensions in distilled water onto a carbon-coated copper grid before drying at room temperature under ambient conditions. All TEM analyses were carried out using a JEOL-100CX microscope operated at 100 kV. All scanning electron microscopy (SEM) images were captured using a field-emission microscope (JSM-7000F, SEI) operated at 10 kV. High-angle annular dark-field (HAADF) images were captured on a UHR FEG-TEM, JEOL JEM-2100F electron microscope using a 200-kV electron source. High-resolution TEM (HRTEM) images and selected-area electron diffraction (SAED) patterns were collected on a JEOL-2011 microscope operated at 300 kV. Powder X-ray diffraction (XRD) patterns were recorded using an Ultima III diffractometer (Rigaku).

Results and discussion

Figure 1a, b shows TEM and SEM images of as-obtained Cu nanostructures synthesized using HDA as sole ligand. The sample was dominated by angular nanocubes ($\sim 50\%$) and nanotetrahedrons ($\sim 50\%$). The size distribution histograms of the Cu nanocrystals (Fig. S1) obtained from the TEM image revealed that the Cu nanocubes had a narrow size distribution with average edge length of ~ 92 nm, while the nanotetrahedrons had a wide size distribution (average edge length 126 nm) due to different standing projections on facet, ridge or vertex. Compared with the nanocrystals synthesized using HDA as sole ligand, Cu nanocubes and nanotetrahedrons with controllable size could be obtained when applying dual ligands (HDA and ODA) at suitable ratios. Typically, when the HDA/ODA mole ratio was 3, monodisperse Cu nanocubes and nanotetrahedrons were obtained with average edge length of 175 and 205 nm, respectively, and the ratio of cubes to tetrahedrons was about 1.5 (Fig. S2). Owing to the relatively narrow size distributions of the Cu nanocubes and nanotetrahedrons, they could be organized

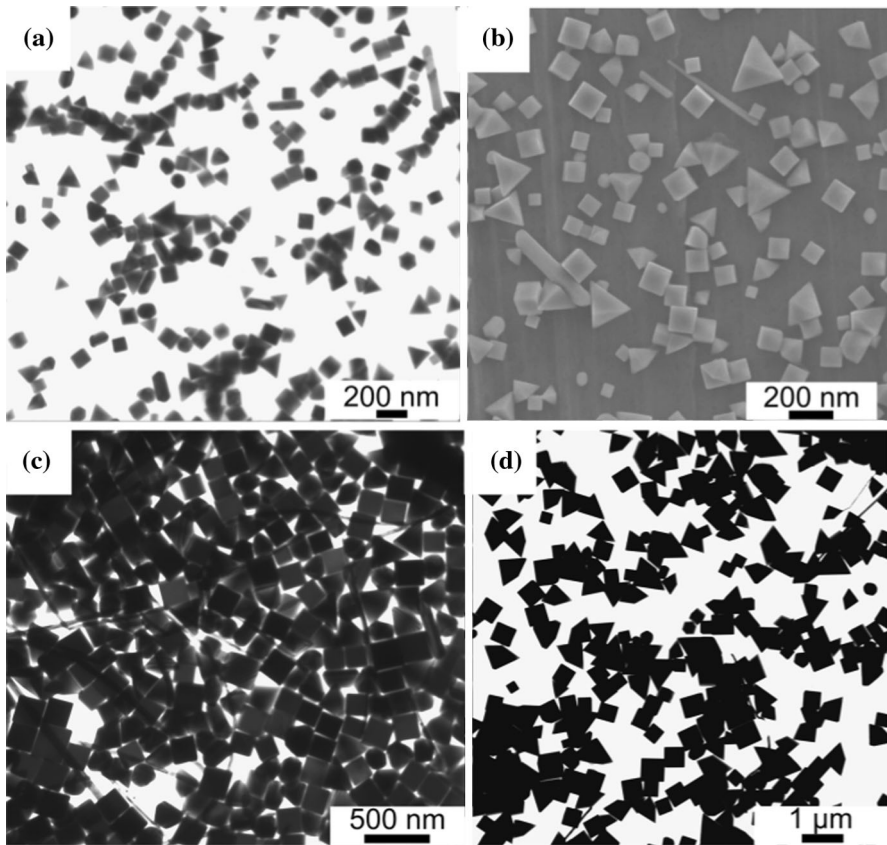


Fig. 1 **a, b** TEM and SEM images of Cu nanocubes and nanotetrahedrons obtained with HDA as sole ligand. TEM images of Cu nanocrystals obtained by HDA and ODA as dual ligands with **c** HDA/ODA = 3 and **d** HDA/ODA = 1/2

into ordered monolayer patterns by evaporating solvent in ambient environment (Fig. 1c). Figure S3a shows the corresponding XRD pattern of the Cu nanocrystals. The strongest diffraction peak is (200) peak, while the (111) diffraction is relatively weak, consistent with the statistical results from the microscope measurements. When the HDA/ODA mole ratio was 1/2, the production of nanocubes and nanotetrahedrons was equivalent. Figure 1d shows a TEM image of Cu nanocrystals with perfect cube and tetrahedron morphology. The average length of the Cu nanocubes and nanotetrahedrons increased to 376 and 536 nm, respectively (Fig. S4). The XRD pattern of the obtained nanocrystals (Fig. S3b) clearly showed that the (111) diffraction was stronger than that of (200), indicating that more nanotetrahedrons were produced in this system.

The microstructure of the obtained nanocrystals was analyzed by HAADF, SAED, and HRTEM. The typical images of a single nanocube or nanotetrahedron shown in Fig. 2 confirm that the nanocrystals had sharp edges and flat facets without any truncations. The SAED pattern of a small-sized nanocube (Fig. 2c) exhibited

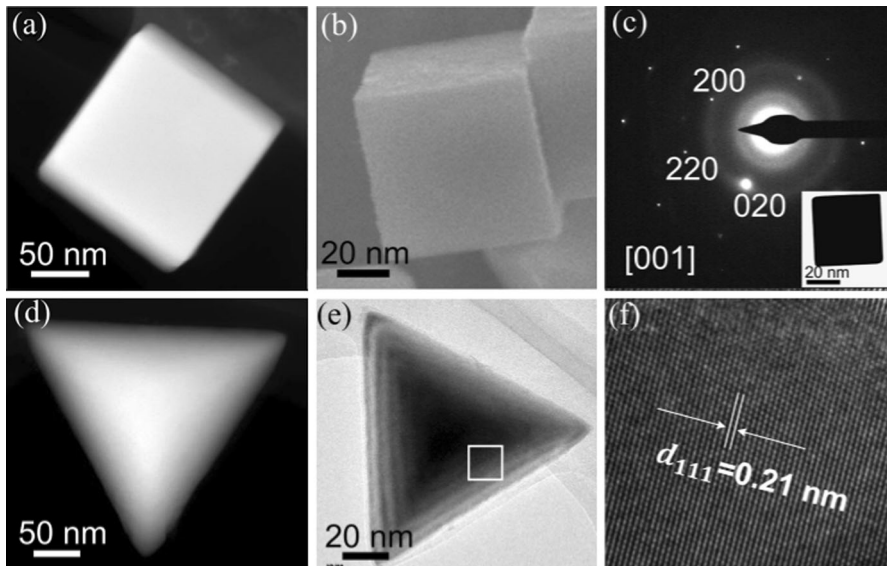


Fig. 2 **a, b** HAADF and SEM images of a single Cu nanocube. **c** SAED pattern of a small-sized Cu nanocube (*inset*) for [001] zone axis. **d, e** HAADF and TEM images of a single Cu nanotetrahedron. **f** HRTEM image of the part labeled in **e**

diffraction spots corresponding to face-centered cubic (fcc)-structured Cu viewed along the [100] zone axis, indicating that the as-prepared Cu nanocubes were single crystals bound by six {100} facets. HAADF and TEM images of one Cu nanotetrahedron are shown in Fig. 2d, e, clearly exhibiting the wedge interference fringe of the incident electron beam. Figure 2f shows a HRTEM image taken from a part of a nanotetrahedron. The well-aligned lattice spacing of 0.21 nm without any defects indicates that the Cu nanotetrahedron was a single crystal covered by four well-defined {111} facets. In addition, SEM and corresponding TEM images of a single tetrahedron were taken from different zone axes with both the SEM and TEM images having the same degree of rotation from -30° to $+30^\circ$, as presented in Fig. 3. They exhibited two different projected shapes: triangle and quadrangle, further confirming the tetrahedron shape of the nanocrystals.

Growth mechanism

The fabrication of the Cu nanopolyhedrons can be divided into two stages: complexation reaction and solvothermal reaction. In the early stage, the growth mechanism of the Cu nanostructures was investigated in detail based on the change of the Cu^{2+} -amine complexes with the presence of HDA and ODA. The observed emulsion color and spectral evolution (Fig. 4) indicated that different Cu^{2+} -amine complexes were indeed formed when changing the type of alkylamine. Furthermore, it was found that the formed Cu^{2+} -amine complexes could control the final morphology of the nanocrystals through altering the complexation reaction

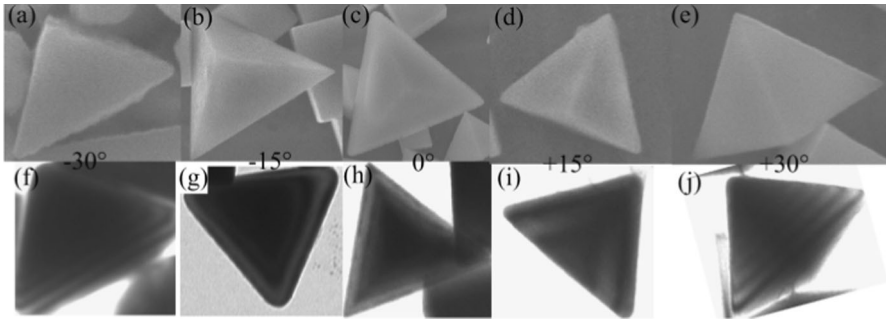


Fig. 3 a–e SEM and f–j corresponding TEM images of a single Cu nanotetrahedron tilted by five different angles from -30° to $+30^\circ$

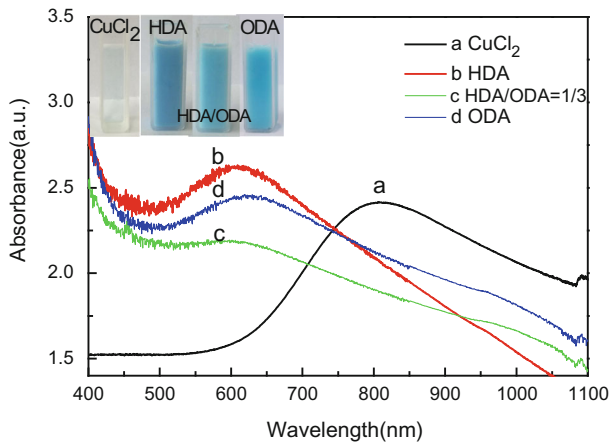


Fig. 4 Emulsion color change and UV–Vis spectra of aqueous Cu salt solution with and without alkylamines

temperature. The complexation reaction proceeded slowly (about 12 h) at room temperature due to the poor solubility of alkylamines at low temperature, and the final products were dominated by Cu nanowires grown from fivefold-twinned seeds (Fig. S5). However, when the complexation reaction temperature was elevated to ~ 323 K, stable Cu^{2+} -amine complexes could form after 5 h due to the improved alkylamine solubility. Then, crystal growth (about 6 h) proceeded quickly, and single-crystalline Cu nanocubes and nanotetrahedrons were the main products in this condition. Therefore, it is proposed that high complexation reaction temperature is suitable for generation of single-crystalline Cu nuclei and their further growth into nanocubes and nanotetrahedrons, while low temperature leads to formation of multitwinned crystal seeds that finally develop into nanowires.

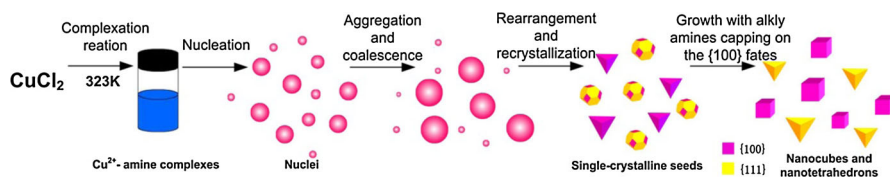
In addition, a series of experiments were carried out in presence of HDA and ODA at different mole ratios. The results (Fig. S6, Table S2) showed that small-sized Cu nanocubes and nanotetrahedrons were obtained when using HDA as sole

ligand, while Cu nanostructures with increasing size were obtained with decreasing HDA/ODA ratio. Relatively large-sized Cu nanocubes and nanotetrahedrons were synthesized when using ODA as sole ligand. This observation confirms that the coordination of Cu^{2+} with ODA is less than that with HDA due to the poor solubility of ODA in water. Therefore, more stable Cu nuclei could be produced in the system with high HDA content, leading to formation of small-sized nanocrystals. Similarly, this helps understand the finding that the size of the Cu nanocubes and nanotetrahedrons increased with decreasing HDA/ODA mole ratio.

In the solvothermal reaction stage, the morphological evolution of the Cu nanostructures can be analyzed based on kinetic and thermodynamic theory. At thermodynamic equilibrium, nanocrystals always grow to have spherical morphology, with their surfaces bounded by lowest-energy, $\{111\}$ facets. Such thermodynamic growth applies for some physical methods, such as chemical vapor deposition under vacuum conditions. However, for colloidal nanocrystal growth, especially when some capping agents are involved in the system, crystal growth is dominated by dynamic factors [33]. For such kinetically controlled structures, aggregative growth has been observed in situ for colloidal nanocrystals such as Au [34], Pt [35], Pd [36], etc. Therefore, it is believed that aggregation and coalescence are also involved in the formation of the Cu nanocubes and nanotetrahedrons. Firstly, Cu^{2+} -amine complexes are reduced by glucose to form Cu nuclei, which rapidly aggregate into stable Cu nanocrystals. Subsequently, structural rearrangement and recrystallization processes occur for the nanocrystals, directing them into single-crystalline Cu nanoseeds with truncated facets. Meanwhile, alkylamines selectively adsorb on the $\{100\}$ facets of these seeds, serving as external confinement for growth of different crystal facets [37]. The area ratio of $\{100\}$ to $\{111\}$ facets depends on the relative growth rate of the two surfaces. When the growth rate ratio of $\{100\}/\{111\}$ is precisely fixed at 0.58, Cu nanocubes without any truncation are formed [38]. In our case, an increase in the area ratio of $\{100\}$ to $\{111\}$ results in the morphology evolution from a triangle-based pyramid to a tetrahedron on adjusting the HDA/ODA mole ratio. The proposed growth mechanism is illustrated in Scheme 1.

Optical properties

Cu nanocubes and nanotetrahedrons can exhibit surface plasmon resonance (SPR) because the dielectric function of Cu has a large negative real component and small imaginary component [39]. Figure 5 shows UV–Vis absorption spectra recorded



Scheme 1 Schematic illustration for aggregative growth of Cu nanopolyhedrons

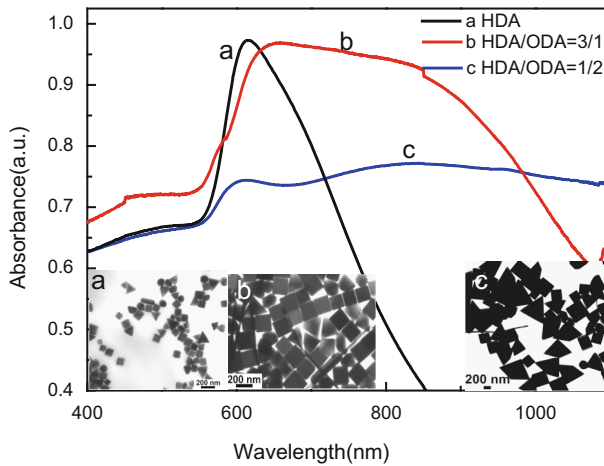


Fig. 5 UV-Vis absorption spectra recorded from aqueous suspensions of monodisperse Cu nanocubes and nanotetrahedrons

from aqueous suspensions of Cu nanocubes and nanotetrahedrons with different edge sizes. When HDA was used as sole ligand, a strong SPR absorption peak at ~ 615 nm (curve a) was observed, along with the corresponding TEM image (image a). The enhanced SPR absorption is mostly due to coherent oscillation of free conduction electrons excited by light within an extremely narrow wavelength region [21]. When using HDA and ODA as dual ligands ($\text{HDA}/\text{ODA} = 3$), there was strong absorption from ~ 590 to ~ 950 nm. Meanwhile, compared with curve a, the SPR peak was red-shifted from ~ 615 to ~ 660 nm (curve b). This red-shift mostly arises from the larger dimension of the Cu nanocubes (175 nm) and nanotetrahedrons (205 nm) compared with the Cu nanocrystals obtained when using HDA as sole ligand (92 and 126 nm for cube and tetrahedron, respectively). Furthermore, when the HDA/ODA mole ratio was 1/2, two SPR absorption peaks appeared at ~ 630 and ~ 840 nm (curve c). This phenomenon was attributed to the fact that the content of nanocubes reduced from about 3/5 to 1/2 while the nanotetrahedrons increased from about 2/5 to 1/2 (see TEM images in Fig. 1c, d).

To identify the origin of these three typical peaks, we performed theoretical [finite-difference time-domain (FDTD)] simulations of the absorption spectra of individual Cu nanocubes and nanotetrahedrons of different sizes. The sizes of the Cu nanocrystals were chosen according to statistical data (Figs. S1, 2, 4) obtained from the TEM images. Figure 6a shows the observed ensemble experimental spectra and a series of FDTD-simulated absorption spectra for individual Cu nanocubes as the edge size is changed from 85 to 105 nm and for nanotetrahedrons from 110 to 130 nm. The intensity of the simulated spectrum was regulated by multiplying by the corresponding proportion according to the statistical data (Fig. S1, 2, 4). Figure 6b, c displays the experimental spectra and corresponding simulated spectra for the other two groups. These results verify that the ensemble experimental spectra are superpositions of the absorption spectra for nanocubes and

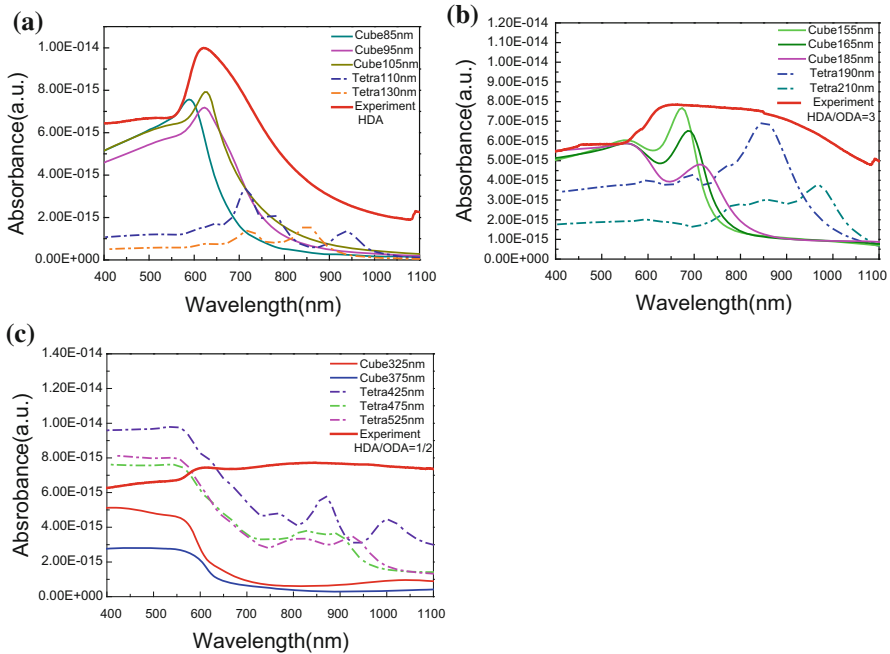


Fig. 6 Experimental absorption spectra and a series of FDTD-simulated absorption spectra for individual Cu nanocubes or nanotetrahedrons: **a** nanocrystals obtained with HDA as sole ligand, and nanocrystals obtained with HDA and ODA as dual ligands with HDA/ODA of **b** 3 and **c** 1/2

nanotetrahedrons in different proportions. Specifically, the peak at about 600 nm in the experimental spectra mainly originates from the Cu nanocubes, while the absorption from 750 to 950 nm is due to the Cu nanotetrahedrons. The discrepancy between the simulated spectra and experimental results can be attributed to the fact that the measured spectra of the Cu nanopolyhedron colloids are average results, while the FDTD simulation results are based on a single Cu nanocrystal. In addition, the difference in the refractive index of the surrounding medium also has a certain impact on the results (actual crystals are sometimes coated by a thin layer of organic matter, while the medium in the FDTD simulation is water).

Since the crystal size is relatively large (from ~ 100 nm to ~ 500 nm), one must also consider the scattering properties of the as-prepared Cu nanocrystals. As shown in Fig. 7a, the absorption spectrum of the solid powder of Cu nanopolyhedrons was similar to that of nanostructures suspended in water, although there is an obvious scattering peak at ~ 600 nm and the scattering intensity gradually increased at long-wavelength regions. In addition, the scattering intensity of the nanocrystals shows a tiny enhancement with increasing average edge length of the Cu nanocrystals, consistent with the scattering spectra simulated using the FDTD method (Fig. 7b).

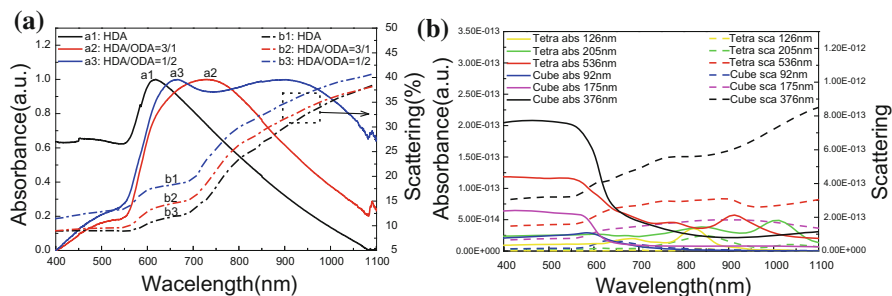


Fig. 7 **a** Absorption and scattering spectra recorded from solid powder of as-prepared Cu nanocubes and nanotetrahedrons. **b** FDTD-simulated absorption and scattering spectra of individual Cu nanocubes with edge size of 92, 175, and 376 nm and nanotetrahedrons with edge size of 126, 205, and 536 nm

Conclusions

We developed a facile method for synthesis of Cu nanopolyhedrons (including nanocubes and nanotetrahedrons) based on hydrothermal reaction in presence of alkylamine. The size of the nanopolyhedrons increased with decreasing HDA/ODA mole ratio. The growth mechanism of the Cu nanocrystals was investigated by changing the complexation reaction temperature and the ligands. By manipulating the concentration of Cu^{2+} -amine complexes, final morphology of nanopolyhedrons or nanowires could be selectively produced. The probable aggregative growth mechanism of these Cu nanocubes and nanotetrahedrons is also discussed. Finally, FDTD simulations revealed that experimental absorption spectra are superpositions of those of nanocubes and nanotetrahedrons in different proportions. The peak at about 600 nm mainly originates from the Cu nanocubes, while the absorption from 750 to 950 nm is due to the Cu nanotetrahedrons. These angular Cu nanocubes and nanotetrahedrons may have promising applications in surface-enhanced Raman scattering and catalysis.

Acknowledgements This project was supported by the National Natural Science Foundation of China (no. 11274173) and the Fundamental Research Funds for the Central Universities (NZ2015101). The work was also sponsored by the Qing Lan Project and Priority Academic Program Development of Jiangsu Higher Education Institutions. Graduate Innovation Base (Laboratory) Open Fund of Nanjing University of Aeronautics and Astronautics, China (kfjj20160803).

References

1. R.L. Keiski, O. Desponds, Y.F. Chang, G.A. Somorjai, *Appl. Catal. A* **101**, 317 (1993)
2. T. Ressler, B. Kniep, I. Kasatkin, R. Schlogl, *Angew. Chem. Int.* **44**, 4704 (2005)
3. A.A. Gokhale, J.A. Dumesic, M. Mavrikakis, *J. Am. Chem. Soc.* **130**, 1402 (2008)
4. S. Vukojević, O. Trapp, J.D. Grunwaldt, C. Kiener, F. Schiith, *Angew. Chem. Int. Ed.* **44**, 7978 (2005)
5. R.R. Wang, H.T. Zhai, T. Wang, X. Wang, Y. Cheng, L.G. Shi, J. Sun, *Nano Res.* **9**, 2138 (2016)
6. C.R. Chu, C. Lee, J. Koo, H.M. Lee, *Nano Res.* **9**, 162 (2016)
7. S. Li, Y. Chen, L. Huang, D. Pan, *Inorg. Chem.* **53**, 4440 (2014)
8. D. Zhang, R. Wang, M. Wen, D. Weng, X. Cui, J. Sun, H. Li, Y. Lu, *J. Am. Chem. Soc.* **134**, 14283 (2012)

9. A.R. Rathmell, B.J. Wiley, *Adv. Mater.* **23**, 4798 (2011)
10. M.A. Ben Aissa, B. Tremblay, A. Andrieux-Ledier, E. Maisonhaute, N. Raouafi, A. Courty, *Nanoscale* **7**, 3189 (2015)
11. M. Blosi, S. Albonetti, M. Dondi, C. Martelli, G. Baldi, *J. Nanopart. Res.* **13**, 127 (2011)
12. W. Li, M.F. Chen, J. Wei, W.J. Li, C. You, *J. Nanopart. Res.* **15**, 1 (2013)
13. L. Li, M.L. Fernández-Cruz, M. Connolly, M. Schuster, J.M. Navas, *J. Nanopart. Res.* **17**, 1 (2015)
14. G. Granata, T. Yamaoka, F. Pagnanelli, A. Fuwa, *J. Nanopart. Res.* **18**, 133 (2016)
15. O.P. Siwach, P. Sen, *J. Nanopart. Res.* **10**, 107 (2008)
16. C. Mayousse, C. Celle, A. Carella, J.P. Simonato, *Nano Res.* **7**, 315 (2014)
17. E. Ye, S.Y. Zhang, S. Liu, M.Y. Han, *Chem. Eur. J.* **17**, 3074 (2011)
18. Y. Chang, M.L. Lye, H.C. Zeng, *Langmuir* **21**, 3746 (2005)
19. M. Mohl, P. Pusztai, A. Kukovecz, Z. Konya, *Langmuir* **26**, 16496 (2010)
20. Y. Sun, F. Zhang, L. Xu, Z. Yina, X. Song, *Mater. Chem. A* **2**, 18583 (2014)
21. H.Z. Guo, Y.Z. Chen, M.B. Cortie, X. Liu, Q.S. Xie, X. Wang, D.L. Peng, *J. Phys. Chem. C* **118**, 9801 (2014)
22. B. Xiao, Z.Q. Niu, Y.G. Wang, W. Jia, J. Shang, L. Zhang, D.S. Wang, Y. Fu, J. Zeng, W. He, K. Wu, L. Jun, J. Yang, L. Liu, Y. Li, *J. Am. Chem. Soc.* **137**, 3791 (2015)
23. S.C. Lu, M.C. Hsiao, M. Yorulmaz, L.Y. Wang, P.Y. Yang, S. Link, W.S. Chang, H.Y. Tuan, *Chem. Mater.* **27**, 8185 (2015)
24. C. Hsia, M. Madasu, M.H. Huang, *Chem. Mater.* **28**, 3073 (2016)
25. C. Wang, H. Daimon, Y. Lee, J. Kim, S. Sun, *J. Am. Chem. Soc.* **129**, 6974 (2007)
26. X.Q. Huang, Y. Chen, C.Y. Chiu, H. Zhang, Y.X. Xu, X.F. Duan, Y. Huang, *Nanoscale* **5**, 6284 (2013)
27. H.Z. Guo, Y.Z. Chen, H.M. Ping, J.R. Jin, D.L. Peng, *Nanoscale* **5**, 2394 (2013)
28. H.J. Yang, S.Y. He, H.L. Chen, H.Y. Tuan, *Chem. Mater.* **26**, 1785 (2014)
29. J. Gu, Y. Guo, Y.Y. Jiang, W. Zhu, Y.S. Xu, Z.Q. Zhao, J.X. Liu, W.X. Li, C.H. Jin, C.H. Yan, Y.W. Zhang, *J. Phys. Chem. C* **119**, 17697 (2015)
30. P. Urchaga, S. Baranton, T.W. Napporn, C. Coutanceau, *Electrocatalysis* **1**, 3 (2010)
31. Z.Q. Niu, Q. Peng, M. Gong, H.P. Rong, Y.D. Li, *Angew. Chem. Int. Ed.* **50**, 6315 (2011)
32. C.X. Kan, C.S. Wang, H.C. Li, J.S. Qi, J.J. Zhu, Z.S. Li, D.N. Shi, *Small* **6**, 1768 (2010)
33. C.X. Kan, J.J. Zhu, X.G. Zhu, *J. Phys. D Appl. Phys.* **41**, 5304 (2008)
34. J.M. Grogan, L. Rotkina, H.H. Bau, *Phys. Rev. E* **83**, 648 (2011)
35. H. Zheng, R.K. Smith, Y.W. Jun, C. Kisielowski, U. Dahmen, A.P. Alivisatos, *Science* **324**, 1309 (2009)
36. L.R. Parent, D.B. Robinson, T.J. Woehl, W.D. Ristenpart, J.E. Evans, N.D. Browning, I. Arslan, *ACS Nano* **6**, 3589 (2012)
37. D.V. Ravi Kumar, I. Kim, Z. Zhong, K. Kim, D. Lee, J. Moon, *Phys. Chem. Chem. Phys.* **16**, 22107 (2014)
38. Z.L. Wang, *J. Phys. Chem. B* **104**, 1153 (2000)
39. E.J. Zeman, G.C. Schatz, *J. Phys. Chem.* **91**, 634 (1987)